Different effects of Ce-doping on orbital and spin ordering in perovskite vanadate $Sm_{1-x}Ce_xVO_3$*

Hu Xin-Bo(胡新波)[a], Hu Ling(胡 令)[a]†, Luo Xuan(罗 轩)[a], Zhao Bang-Chuan(赵邦传)[a], and Sun Yu-Ping(孙玉平)[a][b]‡

[a] *Key Laboratory of Materials Physics, Institute of Solid State Physics, Chinese Academy of Sciences, Hefei* 230031, *China*
[b] *High Magnetic Field Laboratory, Chinese Academy of Sciences, Hefei* 230031, *China*

(Received 25 June 2012; revised manuscript received 28 September 2012)

The effects of Ce-doping on the phase transition of the orbital/spin ordering (OO/SO) are studied through the structural, magnetic, and electrical transport measurements of perovskite vanadate $Sm_{1-x}Ce_xVO_3$. The measurements of structure show that the cell volume decreases as $x \leq 0.05$, and then increases as Ce-doping level increases further. The OO state exists but is suppressed progressively in the sample with $x \leq 0.2$ and disappears as $x > 0.2$. The temperature at which the C-type SO transition is present increases monotonically with Ce-doping level increasing. The temperature dependence of resistivity for each of the samples shows a semiconducting transport behavior and the transport can be well described by the thermal activation model. The activation energy first decreases as $x \leq 0.2$, and then increases for further doping. The obtained results are discussed in terms of the mixed-valent state of the doped-Ce ions.

Keywords: perovskite vanadate, orbital/spin ordering, electrical properties

PACS: 75.25.Dk, 75.30.–m, 75.60.Ej **DOI:** 10.1088/1674-1056/22/4/047501

RVO_3 (R = rare earth elements and Y) compounds have been intensively studied because of their interesting properties, for example, magnetization reversal, electronic phase separation, and magnetic-field-induced switching between two orbital ordered states, etc.[1–3] Each of those phenomena is closely related to orbital/spin orderings (OO/SO), which thus received a lot of attention. A lot of complex interactions and factors are suggested to have influence on the formation of the OO/SO state in vanadate materials, such as Jahn–Teller (JT) coupling, superexchange interaction, covalency effect, orbital fluctuations, random fields, etc.[4–8] Among those factors, the orbital fluctuations and random fields are especially important. Zhou *et al*.[5,6] pointed out that the enhanced orbital fluctuations could cause a remarkable enhancement of the C-type SO state (the temperature at which the C-type SO is present increases considerably). Tung *et al*.[8] suggested that the random fields might be one of the origins of the ferromagnetic component and the magnetization reversal observed in antiferromagnets RVO_3.

In RVO_3 family, $SmVO_3$ and $CeVO_3$ are widely studied due to their interesting OO and SO state. For $SmVO_3$, the G-type OO (GOO) state occurs in the cooling process at about 200 K (T_{OO}), at which an alternating occupation of the d_{xz} and d_{yz} orbitals is found along all three crystal axes. As temperature decreases further, another ordering state (C-type SO) appears at about 130 K (T_{SO}), where the spins of the vanadium ions are antiferromagnetically arranged in ab plane but ferromagnetically arranged along c direction.[2] As for $CeVO_3$, both the transition temperature and the sequence in which the OO/SO is formed have been disputed.[9–12] The valence of Ce ion in $CeVO_3$ is found in the mixed-valent state of Ce^{3+} and Ce^{4+}, and the mixed-valent state may be the possible origin of the anomalous properties observed in $CeVO_3$ system. The OO/SO state is sensitive to the ion substitution at the R-site.[13] In order to further understand the influence of Ce valence state on the physical properties in RVO_3 system, we investigate the effects of the Ce-doping on the OO/SO of perovskite $SmVO_3$ in detail. Our results suggest that Ce-doping weakens the antiferromagnetic (AFM) interaction of spins and suppresses the GOO state, and the GOO in the system was destroyed as Ce-doping level $x > 0.2$. All samples show thermal activation like transport behavior and the sample with $x = 0.2$ has the minimum activation energy. These results are discussed in terms of variation of the Ce^{3+}/Ce^{4+} ratio, the Sm-site size difference and random potential induced by the Ce-doping.

Polycrystalline samples $Sm_{1-x}Ce_xVO_3$ ($0 \leq x \leq 0.4$) are prepared by conventional solid-state reaction method. Appropriate quantities of Sm_2O_3, V_2O_3, and CeO_2 powders are mixed, pelletized, and sealed in evacuated quartz tubes. The quartz tubes are heated at 800 °C, 950 °C for 20 h, and 1100 °C for 60 h with intermediate grindings. Powder X-ray diffraction (XRD) patterns are taken with Cu K_α (λ = 1.5406 Å, 1 Å = 0.1 nm) radiation using a Philips X'pert PRO X-ray diffractometer at room temperature. The magnetization

*Project supported by the National Key Basic Research Program of China (Grant No. 2011CBA00111) and the National Natural Science Foundation of China (Grant Nos. 10974205, 11104273, and 11004193).

†Corresponding author. E-mail: huling@issp.ac.cn
‡Corresponding author. E-mail: ypsun@issp.ac.cn

© 2013 Chinese Physical Society and IOP Publishing Ltd

measurements are performed in a quantum design (QD) superconducting quantum interference device (SQUID) system (1.9 K $\leq T \leq$ 400 K, 0 T $\leq H \leq$ 5 T). Electrical transport measurements are carried out using the four-probe method on a QD physical property measurement system (PPMS, 1.8 K $\leq T \leq$ 400 K, 0 T $\leq H \leq$ 9 T).

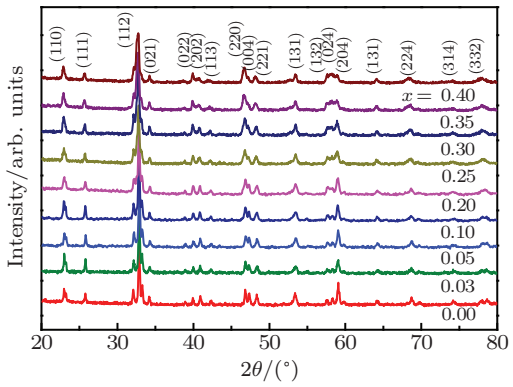


Fig. 1. (color online) Room-temperature powder X-ray diffractions for $Sm_{1-x}Ce_xVO_3$ ($0 \leq x \leq 0.4$) samples.

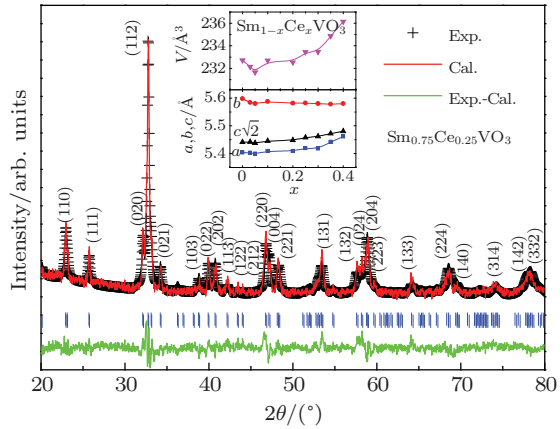


Fig. 2. (color online) The experimental and Rietveld refinement XRD patterns of $Sm_{0.75}Ce_{0.25}VO_3$ sample. Upper inset: the refined cell volume as a function of Ce concentration x. Lower inset: the refined lattice parameter a, b, and c each as a function of Ce doping level x.

Figure 1 shows the room-temperature XRD patterns of $Sm_{1-x}Ce_xVO_3$ ($0 \leq x \leq 0.4$) samples. All the diffraction peaks could be indexed by the orthorhombic structure with *Pbnm* space group and no detectable secondary phase exists. The structural parameters of the samples are refined by the standard Rietveld technique. As an example, figure 2 displays the experimental and Rietveld analysis XRD patterns of $Sm_{0.75}Ce_{0.25}VO_3$ sample. The obtained fitting parameters: the lattice constant a, b, c, and the cell volume V, are plotted each as a function of the Ce-doping level x in the insets of Fig. 2. They show that both a, c, and V decrease first as $x \leq 0.05$, and then increase with Ce-doping level increasing, while b decreases continuously in the whole Ce-doping range. It should be noted that the variation of b parameter is very small compared with those of a and c. The standard ionic radii of Sm^{3+}, Ce^{3+}, and Ce^{4+} are 1.132 Å, 1.196 Å, and 0.97 Å, respectively. According to the non-monotone variation of V with the increase of Ce-doping level x, we suggest that lightly doped Ce ions at Sm-site should mainly be in the form of Ce^{4+} as $x \leq 0.05$. As Ce-doping level $x > 0.05$, both Ce^{3+} and Ce^{4+} ions coexist in the sample and the concentration of Ce^{3+} ions increases monotonically with Ce-doping level increasing. That is to say, Ce ions might be in a mixed-valent state in the heavily Ce-doped samples.

Figure 3 shows the temperature dependences of the magnetization $M(T)$ curves for $Sm_{1-x}Ce_xVO_3$ samples. The data are collected under field-cooling (FC) mode at an applied field of 0.1 T. All FC $M(T)$ curves show sharp upturns with temperature decreasing at a certain temperature T_{SO}, which corresponds to the onset of the C-type SO.[13] The inset of Fig. 3 shows the curves of derivative of $M(T)$ near T_{SO}. As shown there, T_{SO} increases monotonically with Ce-doping level increasing. Figure 4 displays the curves of derivative of $\chi^{-1}(T)$ of $Sm_{1-x}Ce_xVO_3$, and the inset shows the fitting results of $SmVO_3$ according to Curie–Weiss law. For the curves with $x \leq 0.2$, it can be found that there are evident slopes around $T = 200$ K, which were previously reported as signs of the onset of the GOO as temperature decreases.[14,15] The appearance of the slope could be attributed to the quench of the orbital angular momentum when the GOO is formed.[16] As can be seen from Fig. 4, the height of the slope becomes lower as the Ce-doping level increases and almost disappears as x reaches 0.25. It means that Ce-doping can suppress the GOO state in $SmVO_3$ system and the GOO state almost disappears as $x > 0.2$. The magnitude of $d(\chi^{-1}(T))/dT$ in the temperature region above T_{OO} increases slowly as temperature decreases for samples with $x > 0.2$, which might be an indication of the existence of mixed-valent Ce ions as mentioned previously.[17] It should be noted that the substitution of Sm^{3+} ions by Ce^{3+} and Ce^{4+} is random, and the disorder will be induced in the system. In the study of $Eu_{1-x}(La_{0.254}Y_{0.746})_xVO_3$, the size differences in cation-site are increased intentionally and the result shows that GOO is suppressed obviously due to its quasi-one-dimensional confinement.[18] It is also worth noting that a similar phenomenon to disorder-induced melting of the long-range OO state into the short-range correlation has been observed in the hole-doped RVO_3 system.[13] The size variance could be defined as $\sigma^2 = \sum_i (x_i r_i^2 - r_{av}^2)$, where x_i, r_i, and r_{av} are the fractional occupancies, the effective ionic radius of cation, and the averaged ionic radius. At $x = 0.1$, σ^2 for $Sm_{1-x}Ce_xVO_3$ is 1.7×10^{-5} nm^2 on the assumption that the ratio of $Ce^{3+}/Ce^{4+} = 1$, which has the same magnitude as that for $Nd_{0.9}Sr_{0.1}VO_3$.[13] So it is reasonable to infer that the Sm-site size difference is the primary reason for the melting of the

GOO in $Sm_{1-x}Ce_xVO_3$, and in the slightly Ce-doped samples, the disorder only exists in the discontinuous region around the doped Ce ions, and it perhaps has short range correlation before the GOO state is completely destroyed.

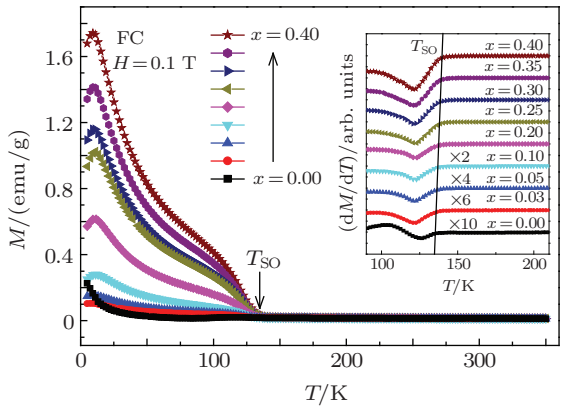


Fig. 3. (color online) Curves of FC magnetization versus temperature with an applied field of $H = 0.1$ T for $Sm_{1-x}Ce_xVO_3$. The inset shows the curves of dM/dT versus T near T_{SO}. The linear line is a guide for the eye.

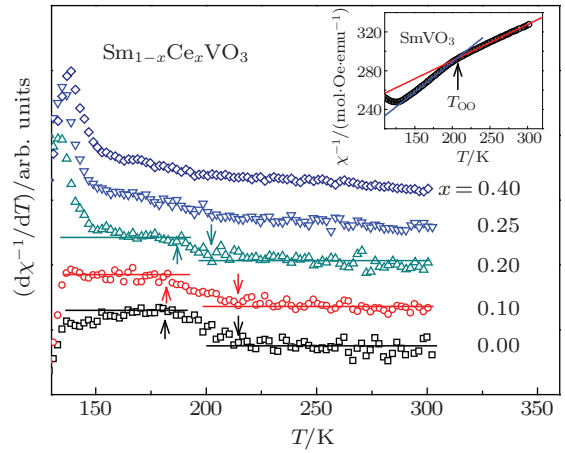


Fig. 4. (color online) Curves of $d\chi^{-1}/dT$ versus T of $Sm_{1-x}Ce_xVO_3$. The lines are guides for the eye. The inset shows the fitting results of $SmVO_3$ according to Curie–Weiss law. The unit 1 Oe=79.5775 A/m.

In order to analyze the variation of the magnetization quantitatively with Ce-doping, all $\chi^{-1}(T)$ curves are fitted to the Curie–Weiss law: $\chi^{-1}(T) = C/(T-\theta)$, where C is the Curie constant and θ is the Weiss temperature. The fitting temperature range above and below T_{OO} are marked as FR_1 (216 K–276 K) and FR_2 (155 K–180 K), respectively. The obtained fitting parameters are listed in Table 1. It can be seen that the value of Curie constant C decreases after the formation of the GOO and the absolute values of θ obtained in both FR_1 and FR_2 range show the same decreasing tendencies. It means that the orbital angular momentum is possibly quenched essentially when the GOO is formed and the AFM interactions in the samples are weakened progressively as Ce-doping level increases.

Table 1. Fitting parameters obtained in different temperature ranges according to the Curie–Weiss law: C_1 and θ_1 in FR_1; C_2 and θ_2 in FR_2.

$x =$	0	0.03	0.05	0.1	0.2	0.25	0.3	0.35	0.4
C_1	2.69	2.56	2.53	2.55	2.30	2.28	2.25	2.22	2.22
C_2	1.59	1.63	1.54	1.63	1.70				
θ_1/K	–576	–517	–532	–496	–421	–376	–358	–348	–323
θ_2/K	–273	–262	–248	–247	–220	–	–	–	–

Another evident characteristic in the $M(T)$ curve is the shift of T_{SO} towards higher temperature as the Ce-doping level increases, implying the enhancement of the C-type SO state. In the studying of $HoVO_3$, Blake *et al.*[4] pointed out that the JT coupling would be completely suppressed when the fluctuations are strong and the total degeneracy of the d_{xz} and d_{yz} orbitals remains below T_{OO}. In our studied samples, the gradual melting of the GOO state could be taken as a sign of the suppression of JT coupling and orbital fluctuations are the dominant force. Zhou *et al.*[5,16] have found that the orbital fluctuations could enhance C-type SO through the studying of $Y_{1-x}La_xVO_3$ and high-pressure effects in RVO_3 system. So we suggest that the enhancement of the C-type SO state in our studied samples could also be attributed to the enhancement of orbital fluctuations.

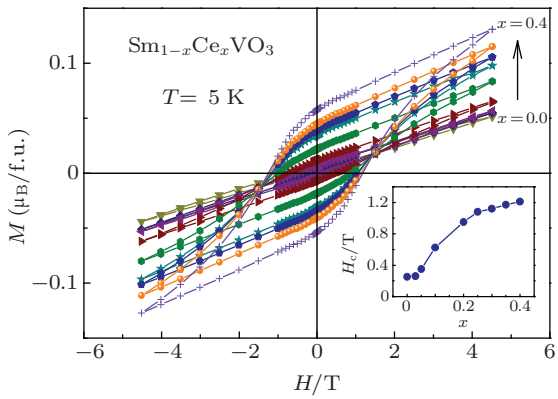


Fig. 5. (color online) Magnetic hysteresis loops of $Sm_{1-x}Ce_xVO_3$ samples at 5 K. The inset shows the Ce-doping level dependence of coercive field H_C.

Figure 5 shows the magnetic hysteresis loops of $Sm_{1-x}Ce_xVO_3$ samples at $T = 5$ K and the inset shows the Ce-doping level dependence of coercive field (H_C). It can be seen that both the magnetic moment and H_C increase as x increases. Tung *et al.*[8] pointed out that the defects in the orbital sector could generate random fields. As mentioned above, the GOO state in the system is suppressed progressively with Ce-doping level increasing. Accordingly, more and more random fields are generated by faulty orbitals as x increases. When the surrounding spins are parallel to the local random fields, additional energy is needed to reverse these spins.[19] Consequently, H_C increases as x increases. On the other hand, the perturbation of random fields may result in a local variation of the AFM arrangement, meaning that the antiparallel spins cannot counteract each other. Thus, AFM interactions are weak-

ened and the magnetic moment is enhanced with Ce-doping level increasing.

Figure 6 shows the temperature dependences of resistivity $\rho(T)$ for $Sm_{1-x}Ce_xVO_3$ samples. In order to study the Ce-doping effects on the transport properties of $Sm_{1-x}Ce_xVO_3$, all $\rho(T)$ curves are fitted by different transport mechanisms and the thermal activation model is found to be the best one. Generally, the thermally activated behavior can be presented as $\rho(T) = \rho_0 \exp[E_a/(k_B T)]$, where E_a, k_B, and ρ_0 are the activation energy, Boltzmann constant, and residual resistivity, respectively. The fitting results are shown in the insets of Fig. 6. It can be found that E_a decreases for $x \leq 0.2$, and then increases as Ce-doping level further increases. This phenomenon might be related to the mixed-valent Ce ions. When $SmVO_3$ is slightly doped with Ce, the concentration ratio of Ce^{3+} to Ce^{4+} ions is relatively small, and E_a decreases because of the effect of band filling. In the heavily Ce-doped samples ($x > 0.2$), the concentration ratio of Ce^{3+} to Ce^{4+} ions increases, meaning that the charge carriers introduced by Ce^{4+} become less and less. So the activation energy increases as Ce-doping level further increases. Another important factor for the increase of activation energy as $x > 0.2$ is the Sm-site size difference. In the study of manganites, a similar phenomenon has been found that cation-size differences can localize charges.[20] The minimum appearing at $x = 0.2$ for E_a is consistent with the critical doping level where the GOO disappears (see Fig. 4). It suggests that the electron scattering from the on-site disorder potential can also account for the increase of E_a for $x > 0.2$.

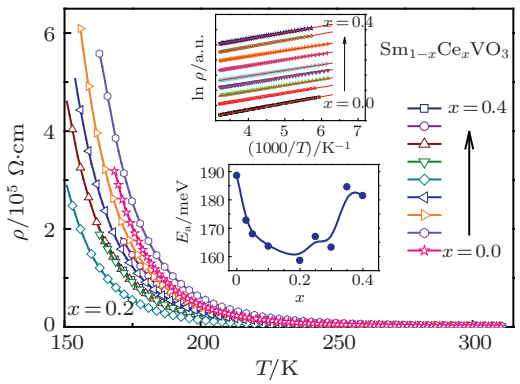


Fig. 6. (color online) Temperature dependences of the resistivity for $Sm_{1-x}Ce_xVO_3$ compounds. Upper inset: $\ln\rho(T)$ versus $1000/T$, the linear lines represent the fitting results according to the thermal activation model. Lower inset: the Ce-doping level dependence of the activation energy E_a.

In conclusion, the effects of the Ce-doping on the structural, magnetic, and electrical transport properties of perovskite vanadate $Sm_{1-x}Ce_xVO_3$ are investigated. The cell volume decreases for $x \leq 0.05$, and then increases, which is suggested to be related to the mixed-valent state of Ce ions. With Ce ions doped into the sample, the GOO state is obviously suppressed and it almost disappears as $x > 0.2$. In contrast, T_{SO} shifts toward higher temperature with Ce-doping level increasing, which is suggested to originate from the enhanced orbital fluctuations. All samples show semiconducting transport behaviors and the transports can be well described by the thermal activation model. The activation energy first decreases and then increases with Ce-doping level increasing, and $x = 0.2$ is the critical point for the activation energy. The obtained results are explained in terms of the mixed-valent state of Ce ions and random fields induced by Ce-doping.

References

[1] Ren Y, Palstra T T M, Khomskii D I, Pellegrin E, Nugroho A A, Menovsky A A and Sawatzky G A 1998 *Nature* **396** 441

[2] Sage M H, Blake G R, Nieuwenhuys G J and Palstra T T M 2006 *Phys. Rev. Lett.* **96** 036401

[3] Miyasaka S, Yasue T, Fujioka J, Yamasaki Y, Okimoto Y, Kumai R, Arima T and Tokura Y 2007 *Phys. Rev. Lett.* **99** 217201

[4] Blake G, Nugroho A A, Gutmann M J and Palstra T T M 2009 *Phys. Rev. B* **79** 045101

[5] Zhou J S, Goodenough J B, Yan J Q and Ren Y 2007 *Phys. Rev. Lett.* **99** 156401

[6] Yan J Q, Zhou J S, Cheng J G, Goodenough J B, Ren Y, Llobet A and McQueeney R J 2011 *Phys. Rev. B* **84** 214405

[7] Bizen D, Nakatsuka K, Murata T, Nakao H and Murakami Y 2008 *Phys. Rev. B* **78** 224104

[8] Tung L D, Lees M R, Balakrishnan G and Paul D McK 2007 *Phys. Rev. B* **75** 104404

[9] Miyasaka S, Okimoto Y, Iwama M and Tokura Y 2003 *Phys. Rev. B* **68** 100406

[10] Ren Y, Nugroho A A, Menovsky A A, Strempfer J, Rütt U, Iga F, Takabatake T and Kimball C W 2003 *Phys. Rev. B* **67** 014107

[11] Muñoz A, Alonso J A, Casáis M T, Martínez-Lope M J, Martínez J L and Fernández-Díaz M T 2003 *Phys. Rev. B* **68** 144429

[12] Reehuis M, Ulrich C, Pattison P, Miyasaka M, Tokura Y and Keimer B 2008 *Eur. Phys. J. B* **64** 27

[13] Fujioka J, Miyasaka S and Tokura Y 2005 *Phys. Rev. B* **72** 024460

[14] Tung L, Lees M R, Balakrishnan G and Paul D McK 2007 *Phys. Rev. B* **76** 064424

[15] Yan J Q, Zhou J S and Goodenough J 2005 *Phys. Rev. B* **72** 094412

[16] Zhou J S, Goodenough J B, Yan J Q, Cheng J G, Matsubayashi K, Uwatoko Y and Ren Y 2009 *Phys. Rev. B* **80** 224422

[17] Kishimoto Y, Kawasaki Y and Ohno T 2003 *Phys. Lett. A* **317** 308

[18] Fukuta R, Miyasaka S, Hemmi K, Tajima S, Kawana D, Ikeuchi K, Yamasaki Y, Nakao A, Nakao H, Murakami Y and Iwasa K 2011 *Phys. Rev. B* **84** 140409

[19] Nattermann T, Shapir Y and Vilfan I 1990 *Phys. Rev. B* **42** 8577

[20] Sundaresan A, Maignan A and Raveau B 1997 *Phys. Rev. B* **56** 5092